Magnetic Field Switching between the Two Orbital-Ordered States in $DyVO_3$

S. Miyasaka,[1,*] T. Yasue,[1] J. Fujioka,[1] Y. Yamasaki,[1] Y. Okimoto,[2,†] R. Kumai,[2] T. Arima,[3,4] and Y. Tokura[1,2,4]

[1]*Department of Applied Physics, University of Tokyo, Tokyo 113-8656, Japan*

[2]*Correlated Electron Research Center (CERC), National Institute of Advanced Industrial Science and Technology (AIST), Tsukuba 305-8562, Japan*

[3]*Institute of Multidisciplinary Research for Advanced Materials, Tohoku University, Sendai 980-8577, Japan*

[4]*Spin Superstructure Project, ERATO, Japan Science and Technology Agency, c/o AIST, Tsukuba 305-8562, Japan*

(Received 5 February 2007; published 19 November 2007)

The critical phase competition between different spin-orbital-ordered states has been investigated for the $DyVO_3$ single crystal. As temperature is lowered, the compound exhibits a reentrant spin and orbital ordering (SO and OO) transition: $C \rightarrow G \rightarrow C$ type for SO and $G \rightarrow C \rightarrow G$ type for OO. It was found that a magnetic field also drives the phase transition from C to G for OO and concomitantly from G to C for SO, the latter of which is coupled with the metamagnetic transition of the Dy $4f$ moments. The mechanism of this novel magnetic-field-induced orbital switching is discussed.

DOI: 10.1103/PhysRevLett.99.217201 PACS numbers: 75.30.Kz, 71.27.+a, 71.30.+h, 75.30.−m

Recent investigations on transition-metal oxides, in particular, colossal magnetoresistive (CMR) manganites [1], have aroused great interest in the interplay among spin, charge, orbital, and lattice degrees of freedom, and orbital ordering (OO) and related phenomena have become important topics in condensed matter physics [2]. In perovskite-type manganites with orbital-active e_g electrons, the charge- or orbital-ordered state competes with the ferromagnetic (FM) metallic one [1,3]. The charge or orbital ordering is melted by external stimuli, such as magnetic and electric fields [1,4] and light/x-ray and electron irradiations [5–7], and consequently the charge- or orbital-ordered insulator to FM metal transition occurs. Perovskite-type RVO_3 (R = rare-earth ion or Y) with orbital-active t_{2g} electrons is another prototypical system with close interplay among spin, orbital, and lattice degrees of freedom. This t_{2g} electron system exhibits two kinds of OO, depending on the R-site ions or temperature (T), and has a possibility of the phase transition between these two long-range orbital-ordered states by external stimuli. Such a controlled switching between the competitive OO states has scarcely been observed apart from one report [8]. The switching of OO means here the phase transition from one orbital-ordered state to another orbital-ordered one, while the melting of OO widely observed in the CMR manganese oxides is the phase transition to the orbital-disordered one. Here we report on the finding of magnetic-field- (H-) induced switching between the orbital-ordered states as well as of the thermally reentrant transition in $DyVO_3$.

Figures 1(a)–1(c) represent the patterns of the spin ordering (SO), OO, and the spin-orbital phase diagram of RVO_3 (R = Tb-Er, Y) [9], respectively. RVO_3 has a $Pbnm$ ($Pnma$) orthorhombic structure with lattice constants of $a \approx b \approx c/\sqrt{2}$ at room T. There are two t_{2g} electrons in V^{3+}. Since the orthorhombic distortion causes a splitting of the energy level of the V^{3+} t_{2g} orbital, one electron always occupies the d_{xy} orbital and the other one either the d_{yz} or the d_{zx} orbital. As T is lowered, RVO_3 (R = Tb-Er, Y) undergoes the structural phase transition from $Pbnm$ orthorhombic to $P2_1/b$ ($P2_1/b$ 1 1) monoclinic form, concomitantly with the G-type OO (G-OO) at T_{OO1}. With further decrease of T, the magnetic transition from a paramagnetic to a C-type antiferromagnetic (AF) state takes place at T_{SO1}. The V^{3+} spins ($S = 1$) are arranged ferromagnetically along the c axis and antiferromagnetically in the ab plane (spin C-type) [10,11], while the occupied d_{yz} and d_{zx} orbitals are staggered in all (x, y, z) directions (orbital G-type) [12,13]. In RVO_3 with R = Y, Ho, and Er, another SO, OO, and lattice structure show up in the lower-T region of $T < T_{OO2} = T_{SO2}$, that is, the G-type SO (G-SO) with the AF coupling between V^{3+} spins, the C-type OO (C-OO) with the alternate $d^1_{xy}d^1_{yz}/d^1_{xy}d^1_{zx}$ electron configuration in the ab plane and the identical one along the c axis, and the $Pbnm$ lattice structure [9–13]. $DyVO_3$ investigated in this study is located in the vicinity of the phase boundary between these two competing spin-orbital-ordered states. To explore the critical features between the competitive SO and OO phases and also the possibility of switching the OO pattern by external stimuli, we have investigated the magnetic, structural, and electronic properties of the $DyVO_3$ single crystal grown by a floating zone method [14].

As shown in Figs. 1(d) and 2(a), the (401) Bragg reflection appears below 195 K ($=T_{OO1}$) in $DyVO_3$. In the $P2_1/b$ monoclinic phase coupled with the G-OO, the Bragg peak of ($h0l$) ($h + l$ = odd), e.g., (401), is allowed, though forbidden in the $Pbnm$ orthorhombic one [13], indicating that the structure is changed from the $Pbnm$ orthorhombic to $P2_1/b$ monoclinic form accompanied by the G-OO below T_{OO1}. With decreasing T, the magnetization (M) [Fig. 1(e)] shows an anomaly due to the magnetic

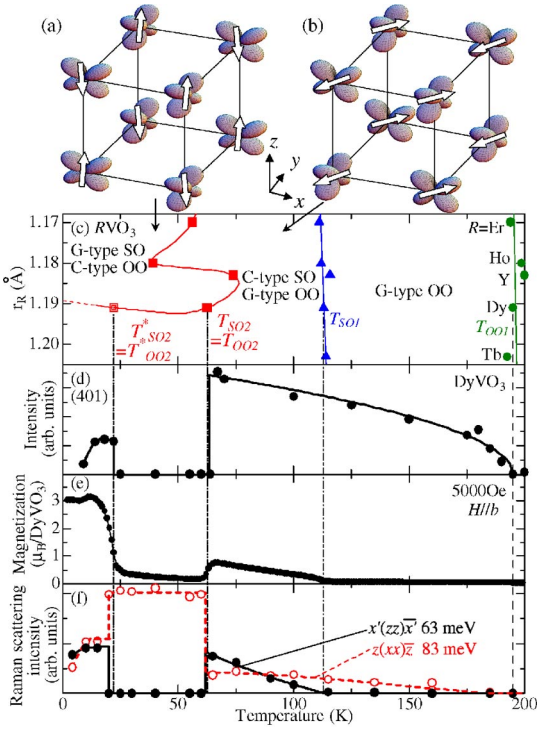

FIG. 1 (color online). (a),(b) The structures of the G-SO and C-OO and the C-SO and G-OO in RVO_3, respectively. Open arrows and lobes indicate spins and occupied d_{yz} and d_{zx} orbitals on V^{3+} ions, respectively. (c) Spin-orbital phase diagram of RVO_3 (R = Tb-Er), where r_R is the R-site ionic radius. Circles, triangles, squares, and double squares indicate T_{OO1}, T_{SO1}, $T_{SO2} = T_{OO2}$, and $T^*_{SO2} = T^*_{OO2}$, respectively. (d) The intensity of the (401) Bragg peak shown in Fig. 2(a). (e) The M and (f) the integrated Raman scattering intensity of the 63 meV two-orbiton band in $x'(zz)\bar{x}'$ polarization (solid circles) and that of the 83 meV phonon band in $z(xx)\bar{z}$ (open circles) shown in Figs. 2(b) and 2(c), for $DyVO_3$. All of the data were measured in a warming run.

transition to the C-type AF state at 112 K ($=T_{SO1}$). The clear fingerprints for the respective SO and OO phases are known to show up in the Raman scattering spectra as the specific phonon modes and the two-orbiton bands [14,15]. We show in Figs. 2(b) and 2(c) the Raman spectra. (Polarization geometry is described using the conventional notation [14]. Optical axes x', y', x, and z are taken parallel to the crystal ones a, b, $a + b$, and c, respectively.) As shown in Figs. 1(f) and 2(b), the 63 meV peak in the $x'(zz)\bar{x}'$ spectrum, which has been assigned to the two-orbiton band in the C-type SO (C-SO) and G-OO phase in RVO_3 [14,15], appears below T_{SO1}. At 64 K ($=T_{SO2} = T_{OO2}$), all of the magnetic, structural, and electronic properties undergo steep changes [Figs. 1(d)–1(f)]. The (401) reflection disappears below T_{SO2}, indicating the structural change from $P2_1/b$ monoclinic to $Pbnm$ orthorhombic. The Raman band around 85 meV in the $z(xx)\bar{z}$ spectrum changes from a two-peak feature to a single-peak one, and the intensity of the 83 meV band, assigned to the oxygen stretching mode coupled with the C-OO [14], is enhanced below T_{SO2} [Figs. 1(f) and 2(c)]. The present results indicate that the OO transition from G-type to C-type occurs concomitantly with the structural transition at T_{SO2} like the other RVO_3 (R = Ho-Lu and Y). The anomaly of M and the disappearance of the two-orbiton band suggest that the AF structure also changes from C-type to G-type. This phase transition at T_{SO2} is of the first order accompanying a large T hysteresis between 57 and 64 K. (See also the corresponding hysteresis of M in $H = 1.0$ T in Fig. 3.) These behaviors in $DyVO_3$ are similar to those in YVO_3 [13,14].

Being distinct from other RVO_3, $DyVO_3$ undergoes another phase transition at a further lower T [16]. The M jumps at 22 K with decreasing T [Fig. 1(e)]. As shown in Figs. 1(d) and 2(a), the (401) Bragg peak revives below 22 K, indicating that this compound undergoes the structural transition from $Pbnm$ orthorhombic to $P2_1/b$ monoclinic again. The spectral features of Raman scattering below 15 K are the same as those between T_{SO2}(= 64 K) and T_{SO1}. Below 15 K, the two-orbiton band appears, and the phonon one assigned to the oxygen stretching mode shows the two-peak structure [Figs. 1(f), 2(b), and 2(c)]. The T dependence of these features shows a hysteresis between 10 and 22 K, indicating the first-order transition. (See Fig. 3.) The present results indicate that $DyVO_3$ undergoes the reentrant transition from the G-type spin- and C-type orbital-ordered (G-spin and C-orbital) state to

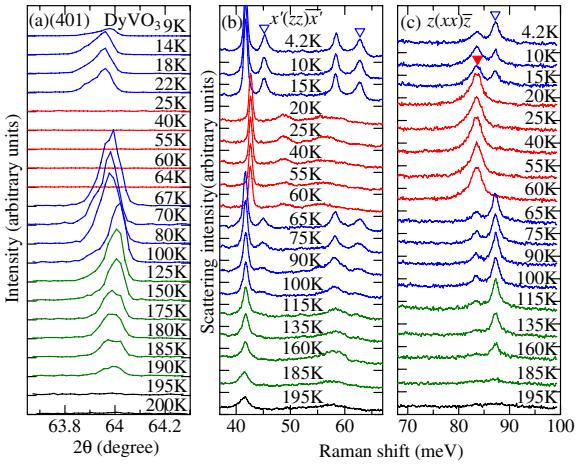

FIG. 2 (color online). (a) Profiles of $\theta - 2\theta$ scan for the (401) Bragg peak, which was observed with use of a synchrotron-radiation x ray (9 keV) at BL-4C, Photon Factory of KEK, and Raman scattering spectra for (b) $x'(zz)\bar{x}'$ and (c) $z(xx)\bar{z}$ polarizations at various temperatures in $DyVO_3$. The 43 and 63 meV peaks in $x'(zz)\bar{x}'$ spectra in the C-spin and G-orbital phase, indicated by the open triangles, are assigned to the two-orbiton excitation, while those around 83 and 86 meV in $z(xx)\bar{z}$ polarization, indicated by solid and open triangles, to the phonon mode activated in the C- and G-orbital states, respectively. The transition T (~22 K) observed by the measurement of Raman scattering is slightly different from that by the x-ray diffraction, due to the local heating (<5 K) on the sample surface by the incident laser.

the C-type spin- and G-type orbital-ordered (C-spin and G-orbital) one at $T^*_{SO2}(= T^*_{OO2} = 10$–$22$ K), as T is decreased. The reentrant SO and OO transition in $DyVO_3$ is likely caused by the critical competition between these two SO and OO affected by the ordering of Dy moments, as discussed later.

The transitions (at T_{SO2} and T^*_{SO2}) between the G-SO/C-OO and C-SO/G-OO phases were found to critically depend on the magnitude of H as well. In Fig. 3, the T-dependent M in $H \parallel a$ and b shows the jump and hysteresis both at higher T_{SO2} and lower T^*_{SO2}. For $H \parallel a$ and b, T_{SO2} and T^*_{SO2} approach each other, and the magnitudes of jump and hysteresis of M at T_{SO2} and T^*_{SO2} reduce with increasing H. Consequently, the first-order phase transition seems to disappear above $H = 2.5$ T applied along the a axis as well as above 3.0 T applied along the b axis, suggesting that in the high H region only the C-spin and G-orbital state subsists below T_{SO1}. At low temperatures, the M is much larger than expected for the V spin of $S = 1$. The Dy $4f$ moment distinctly contributes to the low-T M. As shown in the inset in Fig. 3, the M for $H \parallel a$ and b are easily saturated, and the saturation moments per formula unit are $m^s_a = 4.32$ and $m^s_b = 8.34\mu_B$, respectively. In contrast, the M for $H \parallel c$ monotonously increases up to 14 T. The results indicate that Dy moments lie along either of the two Ising directions within the ab plane, making an angle of about $\pm 27°[= \pm\tan^{-1}(m^s_a/m^s_b)]$ with respect to the b axis.

To clarify the H dependence of SO and OO, we show the M-H curves at various temperatures in Figs. 4(a) and 4(d). Below $T_{SO2}(= 57$–64 K), the M-H curves for $H \parallel a$ and b show the jump and hysteresis, signaling the metamagnetic transition. The large magnitudes of the M and its jump suggest that the anomaly of M is related with the Dy $4f$ moments. As T is lowered, the hysteresis region shifts to the lower H above 10 K. In the both cases for $H \parallel a$ and b, the metamagnetic behavior disappears below 10 K, and the M shows the large nearly saturated value due to the ordered Dy $4f$ moments. (The neutron scattering study has confirmed the FM ordering of the Dy moments below 10 K [17].) On the basis of these observations, the spin-orbital phase diagrams of $DyVO_3$ are shown on the plane of T vs H in Figs. 4(b) and 4(e). All of the anomalies and hysteresis by the magnetic, structural, and OO transition, as observed by the measurements of the T- and H-dependent M [Figs. 3, 4(a), and 4(d)], are plotted in the phase diagrams. The phase diagrams for $H \parallel a$ and b are similar apart from a difference in the hysteretic regions: the intermediate-T C-orbital and G-spin state changes to the G-orbital and C-spin one, as H is increased above 3–4 T. In Figs. 4(b) and 4(e), $T_{SO2} = T_{OO2}$ connects with $T^*_{SO2} = T^*_{OO2}$ in the high H region. In contrast with the cases of $H \parallel a$ and b, no sign of the metamagnetic transition nor the H-induced switching between the two types of SO and OO was observed when the H up to 14 T is applied to the c axis.

The measurements of the Raman scattering spectra with use of a superconducting magnet (generating H up to 5 T) confirmed the present conclusion. First, the crystal with the surface of the bc ($y'z$) plane was cooled down to 65 K in zero H, and the $x'(zz)\bar{x}'$ spectrum was measured. As shown in Fig. 4(c), the spectrum shows the two-orbiton bands

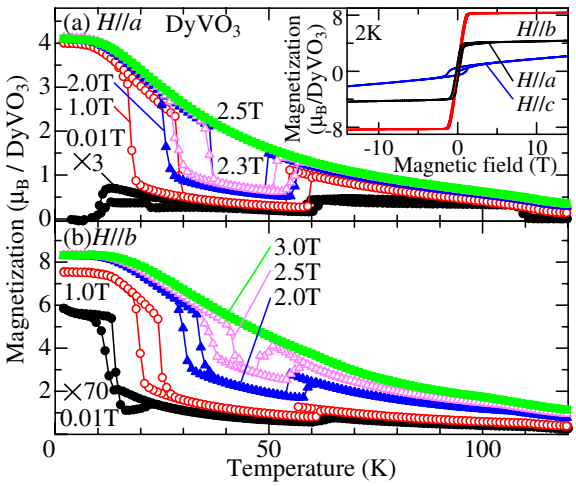

FIG. 3 (color online). T dependence of M in H applied parallel to (a) the a axis and to (b) the b axis in $DyVO_3$. All of the measurements were performed in the process of the H cooling and then warming. The inset presents the M-H curves for $H \parallel a$, b, and c axes at 2 K, respectively.

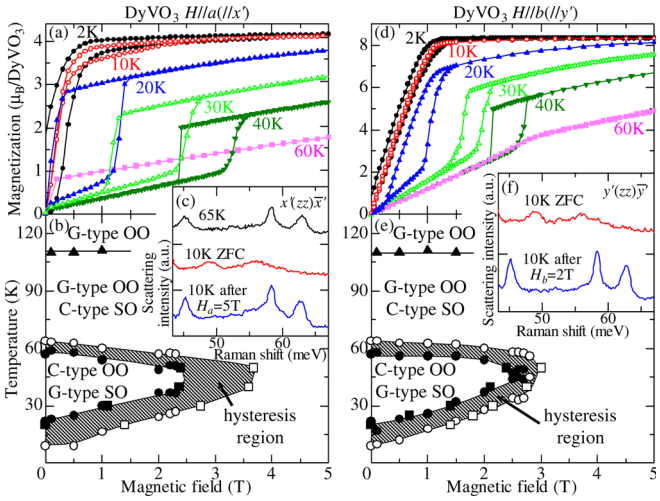

FIG. 4 (color online). (a)–(c) show the results for $H \parallel a$ (x') and (d)–(f) for $H \parallel b$ (y'). (a),(d) The H dependence of M was measured after zero-H cooling (ZFC). (b),(e) The spin-orbital phase diagram in the plane of T and H. Triangles and circles/squares represent T_{SO1} and $T_{SO2} = T_{OO2}$ ($T^*_{SO2} = T^*_{OO2}$), respectively. The data indicated by circles and squares were obtained by cooling and warming and H-increasing and decreasing runs, respectively. Hatched areas indicate the hysteresis region. (c),(f) The Raman scattering spectra indicated as 65 and 10 K ZFC were measured at respective temperatures after ZFC. At 10 K, H is applied along the a or b axis and then removed. After this procedure, the spectra, indicated as 10 K after $H_a = 5$ T or $H_b = 2$ T, were measured.

characteristic of the C-SO and G-OO phase. The crystal was further cooled down to 10 K under zero H, and the $x'(zz)\bar{x}'$ spectrum was measured again. In this procedure, the sample has passed the intermediate-T G-SO and C-OO phase and finally reached the hysteresis region in Fig. 4(b). Therefore, the spectrum at 10 K shows the spectral feature characteristic of the G-spin and C-orbital state. At 10 K, $H = 5$ T was applied along the a axis and then decreased to zero. This H-scanning procedure corresponds to the traverse of the phase boundary to the higher-H phase and then returning to the hysteretic region at $H = 0$. As shown in Fig. 4(c), the Raman spectrum after removing H is identical to that in the C-spin and G-orbital state above the higher T_{SO2}, e.g., showing the two-orbiton bands. A similar procedure and measurements have been performed for $H \parallel b$ axis. The Raman spectrum shows the characteristic of the G-SO and C-OO phase after the zero-H cooling down to 10 K, while that at 10 K shows the two-orbiton bands after applying and then removing the H of 2 T. These results have confirmed that the electronic state realized in the higher H applied along the a or b axis is spin C-type and orbital G-type.

The origin of the thermally reentrant and H-induced phase transitions between the two types of spin-orbital-ordered states can be assigned to the exchange coupling between the V d spins and Dy f moments. With the consideration of the variation in Dy-V distance ($d \approx 0.333$ nm) in the actual lattice structures of the respective phases, it can be shown that the exchange interaction (J_{f-d}) between the Dy and V moments (S_{Dy} and S_{V}, respectively) favors energetically the C-spin state rather than the G-spin state, when the two states are otherwise degenerate in free energy. The atomic position and lattice parameters of $DyVO_3$ at 30 (C-orbital state) and 70 K (G-orbital state), determined by the analysis of the single crystal x-ray diffraction, have been used for the following calculation [18]. The energy gain of the G-orbital and C-spin state relative to the C-orbital and G-spin state approximately amounts to $1 \times 10^{-5}(\partial J_{f-d}/\partial d)|S_{\mathrm{Dy}}||S_{\mathrm{V}}|d$ per unit cell, if only the d dependence of J_{f-d} is explicitly taken into account. J_{f-d} usually on a small energy scale is likely to be determinant in the present case of the critical phase competition. At $H = 0$, the FM state of Dy moments sets in below 20 K, where the C-spin and hence G-orbital state reentrantly emerges. A similar situation can occur even at $T > 20$ K, when the metamagnetic transition of the Dy moments is induced by H applied along either the a or the b axis. (Note here that Dy moment easy axes lie within the ab plane.) As a result, the high-H spin-orbital-ordered state should be always the spin C-type and orbital G-type, as observed in the phase diagrams [Figs. 4(b) and 4(e)]. While the important interplay between f and d moments have been known for some perovskites [19–21], the present work has thus demonstrated the clear evidence that the orbital-ordered patterns and related electronic properties can be also controlled by the external H through the f-d interactions and the strong coupling between the SO and OO.

In summary, the critical features near the phase boundary between two types of spin- and orbital-ordered states in $DyVO_3$ have been investigated by the measurements of M, Raman scattering spectra, and x-ray diffraction. With decreasing T, the spin- and orbital-ordered patterns in $DyVO_3$ show the reentrant change, $C \rightarrow G \rightarrow C$ type and $G \rightarrow C \rightarrow G$ type, respectively, as triggered by the FM ordering of Dy Ising moments coupled with the V $3d$ spins. In the intermediate-T region (10–22 K $< T <$ 57–64 K), the H along the a and b axes induces the metamagnetic transition of the Dy Ising moments. The H alignment of Dy $4f$ moment causes the rearrangement of V^{3+} spins from G-type to C-type via the f-d spin exchange interaction and accordingly the switching of the pattern of occupied d_{yz}/d_{zx} orbitals from C-type to G-type.

We thank S. Onoda, Y. Motome, N. Nagaosa, C. Ulrich, and B. Keimer for helpful discussions. This work was supported by KAKENHI (No. 18740192, No. 17340104, No. 16076207, and No. 15104006) and TOKUTEI (No. 16076205) from JSPS and MEXT.

*Present address: Department of Physics, Osaka University, Osaka 560-0043, Japan.

†Present address: Department of Materials Science, Tokyo Institute of Technology, Tokyo 152-8551, Japan.

[1] Y. Tokura, Rep. Prog. Phys. **69**, 797 (2006).
[2] Y. Tokura and N. Nagaosa, Science **288**, 462 (2000).
[3] Y. Tomioka and Y. Tokura, Phys. Rev. B **70**, 014432 (2004).
[4] A. Asamitsu *et al.*, Nature (London) **388**, 50 (1997).
[5] V. Kiryukhin *et al.*, Nature (London) **386**, 813 (1997).
[6] K. Miyano *et al.*, Phys. Rev. Lett. **78**, 4257 (1997).
[7] M. Hervieu *et al.*, Phys. Rev. B **60**, R726 (1999).
[8] K. Hatsuda, T. Kimura, and Y. Tokura, Appl. Phys. Lett. **83**, 3329 (2003).
[9] S. Miyasaka *et al.*, Phys. Rev. B **68**, 100406 (2003).
[10] C. Ulrich *et al.*, Phys. Rev. Lett. **91**, 257202 (2003).
[11] M. Reehuis *et al.*, Phys. Rev. B **73**, 094440 (2006).
[12] M. Noguchi *et al.*, Phys. Rev. B **62**, R9271 (2000).
[13] G. R. Blake *et al.*, Phys. Rev. Lett. **87**, 245501 (2001).
[14] S. Miyasaka *et al.*, Phys. Rev. B **73**, 224436 (2006).
[15] S. Miyasaka *et al.*, Phys. Rev. Lett. **94**, 076405 (2005).
[16] In the phase diagram of Ref. [9], the phase transition around 10–22 K for $DyVO_3$ is not displayed. In Ref. [9], we thought that the anomaly of M around 10–22 K was caused only by the magnetic ordering of Dy moments and not by the change of the SO and OO of V ions.
[17] C. Ulrich and B. Keimer (unpublished).
[18] See EPAPS Document No. E-PRLTAO-99-052747 for a table of the results of the structure refinements. For more information on EPAPS, see http://www.aip.org/pubservs/epaps.html.
[19] T. Kimura *et al.*, Nature (London) **426**, 55 (2003).
[20] J. E. Bouree and J. Hammann, J. Phys. (Paris) **36**, 391 (1975).
[21] R. Bidaux, J. E. Bouree, and J. Hammann, J. Phys. (Paris) **36**, 803 (1975).